Impact of the surface chemistry of 2D nanoplatelets on cation exchange

Lina Makké, Ningyuan Fu, Henri Lehouelleur, Hong Po, Corentin Dabard, Leonardo Curti, Erwan Bossavit, Xiang Zhen Xu, Gilles Patriarche, Debora Pierucci, et al.

Impact of the surface chemistry of 2D nanoplatelets on cation exchange

Lina Makké[1], Ningyuan Fu[1], Henri Lehouelleur[1], Hong Po[1], Corentin Dabard[1], Leonardo Curti[1], Erwan Bossavit[2], Xiang Zhen Xu[1], Gilles Patriarche[3], Debora Pierucci[4], Mathieu G. Silly[2], Emmanuel Lhuillier[4], Sandrine Ithurria[1*]

[1] Laboratoire de Physique et d'Etude des Matériaux, ESPCI-Paris, PSL Research University, Sorbonne Université Univ Paris 06, CNRS UMR 8213, 10 rue Vauquelin 75005 Paris, France.
[2] Synchrotron SOLEIL, L'Orme des Merisiers, Départementale 128, 91190 Saint-Aubin, France.
[3] Université Paris-Saclay, CNRS, Centre de Nanosciences et de Nanotechnologies, 91120, Palaiseau, France
[4] Sorbonne Université, CNRS, Institut des NanoSciences de Paris, INSP, F-75005 Paris, France.

Abstract: Among nanocrystals, 2D zinc blende nanoplatelets (NPLs) provide the highest level of growth control, resulting in sub-monolayer roughness on their surface and hence on their thickness. This characteristic enables a uniquely narrow spectral linewidth. The synthesis of 2D particles is now well controlled with cadmium chalcogenides but the growth process remains difficult to extend to other materials. Therefore, an alternative strategy to achieve a roughness-free 2D object is to perform cation exchange on as-synthesized NPLs. Nevertheless, if not properly conducted, this strategy leads to dramatic shape reconstruction, resulting in the loss of beneficial properties. Here, we demonstrate that surface chemistry can significantly impact the kinetic and thermodynamic properties of the cation exchange procedure. When performing copper exchange on CdSe NPLs, we find that thiols are the most suitable ligands for shape preservation. This can be attributed to the ligand-induced lattice contraction on CdSe, which minimizes lattice distortion during cation exchange. Conversely, we determine that the initial flatness of the particle, ligand length, and ligand binding strength are not critical for maintaining the shape, although they impact the reaction duration. Finally, the method is generalized to multiple CdSe thicknesses and to CdS NPLs.

*To whom correspondence should be sent: sandrine.ithurria@espci.fr

INTRODUCTION

Colloidal nanocrystals (NCs) have become a versatile platform for optoelectronics owing to the combination of a broad spectral tunability through quantum confinement and an extensive range of materials. A key advantage of these NCs over existing light-sources is their inherent robustness, along with their ability to achieve narrow emission. This characteristic, generally driven by low size dispersity, is particularly valuable in display applications, where achieving a narrow green emission is a critical requirement to reach a wide gamut.[1] Now, thanks to almost 40 years of chemical optimization, size and shape can also be well controlled. Among best-controlled materials in the Infrared, PbS reaches nearly monolayer accuracy corresponding to a size dispersion below 5%.[2,3] And among colloidal nanocrystals, 2D Nanoplatelets[4] (NPLs) achieve the narrowest tunable spectral emissions. In such NPLs, the narrowness of the optical features arises from the specific growth mechanism that enables a roughness-free surface over thousands of nm^2. Other 2D materials grown through other mechanisms do not inherently present narrow linewidths. An illustration of that is PbS. A synthesis using lead-octadecyl-xanthate as a precursor has been reported and enables the growth of PbS NPLs showing emission linewidth narrower than their spherical counterparts but non tunable optical properties[5]. Other syntheses have been proposed but the obtained 2D particles present PL linewidth similar to those obtained for 0D NCs.[6–9] Thus, to achieve sub-monolayer control on growth, either a new synthetic path has to be discovered, or materials such as cadmium chalcogenides NPLs can be used as templates. In this latter case, a cation exchange can be performed as a way to change the composition.[10–14] This process has first been introduced on nanocrystals 20 years ago and has appeared to be an interesting strategy to synthesize nanoparticles of shape, composition and crystal phases which are not feasible yet by direct synthesis.[15–20] The goal is to preserve the anionic sublattice while exchanging the cationic framework in order to preserve the shape of the particles and in some extend the crystal structure.[21,22] The first demonstrations were on CdSe exchanged with Cu^+, but have been widely extended up to the formation of InP from Cu_3P or InAs from Cu_3As.[23,24] Another successful cation exchange has been achieved with mercury chalcogenides[10–12,25,26] to obtain near-infrared active 2D NPLs with a topotaxial cation exchange, where both the host and final NPLs present the same zinc blende cubic crystal structure.

In general, conducting a cation exchange process is particularly tricky on non-spherical shapes, especially if one of the dimensions is of the order of 1 to 2 nm and if the targeted materials present a thermodynamically stable phase different from the host materials.[14,15,27,28] During the process, while the native cations are replaced by the new ones, the anion sublattice can be destabilize leading to a shape reconstruction or a change in the anionic sublattice.[15,29] However, it is critical to avoid shape reconstruction to maintain a reduced surface roughness and thus to obtain optimal optical features. As sake of illustration, Dabard *et al.* pointed out that a slow cation exchange (conducted at low temperature and using bulky precursor) is critical to obtain 2D HgTe NPLs,[10] maintaining the shape of the initial particle. Since the precursor and nanoparticle surface chemistry strongly impact the exchange dynamics,[30,31] it becomes critical to rationally study how the surface chemistry of NPLs affects the cation exchange process. In this paper, we focus on the model case of CdSe NPLs experiencing a copper cation exchange.[22,32] We systematically study the effect of the nature of capping ligands, the impact of ligands coverage as well as the length of the aliphatic chain of ligands. Finally, we generalize the results to NPLs of different thicknesses and to other cadmium chalcogenide NPLs.

METHODS

Chemicals: octadecene (ODE, Thermo Scientific, 90%), cadmium acetate anhydrous ($Cd(Ac)_2$, Sigma-Aldrich, 99.995%), cadmium acetate dihydrate ($Cd(Ac)_2.2H_2O$, Sigma-Aldrich, 98%), cadmium oxide (CdO, Strem 99.99%), cadmium bromide tetrahydrate ($CdBr_2.4H_2O$, Aldrich, 98%), cadmium iodide (CdI_2, Aldrich, 99%), cadmium nitrate tetrahydrate ($Cd(NO_3)_2.4H_2O$, Sigma-Aldrich, 98%), myristic acid (Fluka, >98%), Acetic Acid (Sigma-Aldrich, >99.7%), sulfur (S, Sigma-Aldrich, >99.0%), selenium (Se, Strem Chemicals 99.99%), sodium borohydride ($NaBH_4$, Aldrich, >98%), tetrakis(acetonitrile)copper (I) hexafluorophosphate ($[Cu(CH_3CN)_4]PF_6$, Sigma-Aldrich, 97%), oleic acid (OA, Alfa Aesar, 90%), tributylphosphine (TBP, Cytec), trioctylphosphine (TOP, Alpha Aesar, 90%), ethanethiol (Aldrich, 97%), butanethiol (Sigma-Aldrich, 99%), octanethiol (Fluka, >97%), dodecanethiol (Sigma-Aldrich, 98%), octadecanethiol (Aldrich, 98%), oleylamine

(OLA, Acros, 80-90%), n-hexane (VWR, 99%), ethanol (VWR, 96%), methanol (VWR), toluene (VWR), toluene anhydrous (Sigma-Aldrich, 99.8%), methanol anhydrous (Sigma-Aldrich, 99.8%), diethyl ether (VWR), tetrahydrofuran (THF) (VWR), N-methylformamide (NMF) (Sigma-Aldrich, 99,8%), isopropanol (VWR), acetone (VWR), tetrachloroethylene (TCE) (Uvasol). All chemicals are used as received.

1 M TOP:Se precursor: In a glovebox, 1.58 g of Se powder is mixed with 20 mL of TOP. The mixture is stirred overnight and is stored in the glovebox for further use.

Cadmium myristate ($Cd(Myr)_2$): In a 50 mL three-neck flask, 11 g of myristic acid and 2.56 g of CdO are mixed and degassed at 80 °C for 30 min. Then under argon flow, the temperature is set at 200 °C. The mixture is heated until the solution becomes colorless (around 40 min). The solution is then cooled down and 30 mL of methanol is added at 60 °C. The solid is washed five times by centrifugation in methanol. The final cadmium myristate is dried under vacuum at 70 °C overnight.

1 M octadecanethiol solution: 2.86 g of octadecanethiol is dissolved in 10 mL toluene. The solution is sonicated for 10 min and ready to use right away.

0.5 M $Cd(X)_2$ (X=I, Br) solution: 458 mg of CdI_2 is dissolved in 2.5 mL methanol. Identically, 430 mg of $Cd(Br)_2$ is dissolved in 2.5 mL methanol. Both solutions were sonicated for 5 min.

2 ML CdSe NPLs synthesis: In a 50 mL three-neck flask, 160 µL of OA and 260 mg of $Cd(Ac)_2.2H_2O$ are added to 20 mL ODE. The mixture is degassed at room temperature for 1 hour and then the atmosphere is switched to argon. The temperature is set to 160 °C and a solution of 250 µL TOP:Se (1M) mixed with 500 µL of ODE is injected at 120 °C. The reaction mixture is reacted at 120 °C for 1 hour and then is cooled down to room temperature. At 150 °C, 2 mL of OA is added. The NPLs are washed using a mixture of hexane and ethanol in equal volumes and this washing step is repeated twice with a reduced amount of ethanol (using a volume ratio of 2:1 volume for hexane to ethanol). Finally, the NPLs are redispersed in 10 mL hexane.

3 ML CdSe NPLs synthesis: In a 50 mL three-neck flask, 260 mg $Cd(Ac)_2.2H_2O$ and 200 µL OA are added to 15 mL ODE and the mixture is degassed at 60 °C for 30 min. The atmosphere is then switched to argon and the temperature is set at 190 °C. At 185 °C, a solution of 600 µL TOP:Se (1 M) diluted with 5.4 mL of ODE is injected at a controlled rate of 9 $mL.h^{-1}$. At the end of the injection, the solution is cooled down to room temperature and the NPLs are precipitated using a mixture of hexane and ethanol in equal volumes. The washing is repeated twice using a minimum of ethanol (using a volume ratio of 2:1 volume for hexane to ethanol). Finally, the NPLs are redispersed into 10 mL hexane. Considering that all the Se precursors reacted (introduced by default), in the suspension of 3 ML CdSe NPLs, the concentration of Cd is 80 mM.

4 ML CdSe NPLs synthesis: In a 50 mL three-neck flask, 340 mg of $Cd(Myr)_2$, 24 mg of Se powder and 25 mL of ODE are added. After 20 min degassing at room temperature, the atmosphere is switched to argon and the temperature is set at 230 °C. When the color turns deep orange, (around 203 °C), 110 mg of $Cd(OAc)_2.2H_2O$ are swiftly added. The solution is heated for 15 min more and then cooled down to room temperature. At 150 °C, 500 µL of OA is added. Then, the obtained solution is precipitated using 20 mL of hexane and 30 mL of ethanol. The obtained pellets are redispersed in 10 mL of hexane and precipitated a second time using 10 mL of ethanol. The final NPLs are redispersed in 10 mL of hexane. Considering that half of the Se introduced is lost in the formation of QDs byproducts, in the suspension of NPLs the concentration of Cd is 18.7 mM.

4 ML CdSe lateral extension: From the solution of 4ML CdSe NPLs, 2mL are precipitated and redispersed in 6mL ODE, and placed in a 50mL three necked flask. To that is added 201mg of $Cd(Ac)_2$, $2H_2O$ and 300µL OA. The mixture is heated to 100°C and placed under vacuum for 1hour. After the degassing step, the solution is placed under Argon atmosphere and heated to 230°C. At that temperature, a mixture of 170µL TOPSe (1M), 100µL Acetic Acid and 3,57mL ODE is injected at a controlled rate of 1mL/h. At the end of the injection, the reaction medium is removed from the heating mantle and 1mL OA is

added at 150°C. Washing step is carried out using a mixture of Hexane and Ethanol in equal proportions and repeated two times using less Ethanol. The final product is redispersed in 10mL Hexane. Considering that all the Se precursors reacted (introduced by default), in the suspension of NPLs, the concentration of Cd is 50 mM.

5 ML CdSe NPLs synthesis: Large 5 ML CdSe NPLs are obtained while growing one layer of CdSe by Colloidal Atomic Layer deposition (c-ALD) on 3 ML CdSe NPLs. In a centrifugation tube, 2 mL of 3 ML CdSe NPLs were introduced along with a few drops of ethanol and 20 µL TBP. Separately, 40 mg of $NaBH_4$ is dissolved in 500 µL NMF and 500 µL ethanol. To the solution is added, at once, 24 mg of Se powder. Once fully transparent, 500 µL of the previous solution is added to the 3 ML NPLs and the tube is shaken until full precipitation of the NPLs into orange aggregates. The solid precipitate is redispersed in 5 mL NMF to facilitate its separation from the transparent hexane phase and 5 mL hexane; few drops of ethanol and 20 µL TBP are added again for a complete washing. This step is repeated at least two times. The retrieved NMF solution is centrifuged with the addition of 5 mL toluene and the NPLs precipitate is redispersed in 5 mL NMF with 37 mg of $Cd(Ac)_2.2H_2O$. Finally, 5-8 mL hexane was added and the NPLs were transferred to the hexane phase with the addition of 1 mL OA and 2 mL methanol. This is observed by a color shift of the lower phase from red-orange to transparent and the upper phase from transparent to red-orange simultaneously. The hexane phase is collected and centrifuged with the addition of ethanol. For the final step, the NPLs are redispersed in 3 mL ODE and added to a 25 mL three-neck flask containing 25 mg of $Cd(Ac)_2.2H_2O$, 40 µL of TBP, and 35 µL of OA. The mixture is degassed at 50 °C for 20 min after which the atmosphere is switched to argon and the temperature is set to 225 °C. The solution is left at the set temperature for 20 min and then cooled down to room temperature. The NPLs are precipitated using a mixture of hexane and ethanol in equal volumes. The washing step is repeated two times and the NPLs are redispersed in 10 mL of hexane. Considering that all the initial 3 ML NPLs properly reacted to c-ALD, the concentration of Cd in the final solution is 24 mM.

4 ML CdS synthesis: In a three-neck flask, 106.6 mg of $Cd(Ac)_2.2H_2O$, 1mL of a solution of S in ODE (0.1 M) and 127 µL of OA are mixed with 7.6 mL ODE and placed under vacuum at room temperature for 10 min. After switching to argon atmosphere, the solution is heated to 250 °C and kept at this temperature for no more than 1 min. Finally, the solution is cooled down to room temperature and washed with hexane and ethanol in equal volumes. The washing step is repeated two times and the final product is suspended in 5 mL of hexane. The final solution is estimated to have 25mM in Cd.

Ligand exchange (from carboxylates to thiolates): Adapted from ref[33] For each population of NPLs, a quantity equivalent to 0.08 mmol of total cadmium in the NPLs is used. The NPLs are precipitated with the addition of a few drops of ethanol and redispersed in 5 mL of toluene. To these solutions, the desired thiol is added in order to have n_{thiol} (mol) : $n_{Cd(surface)}$ (mol) = 100 : 1 (with $n_{Cd(surface)} = (n_{Cd(tot)}.2)/(N+1)$ and N the number Se monolayers). The thiols used are ethanethiol, butanethiol, octanethiol, dodecanethiol, octadecanethiol. The mixture is left to react for 2 days under constant stirring at room temperature (~ 22 °C), after which the NPLs were precipitated via centrifugation without the use of additional solvent. The completion of the exchange is monitored through a shift of the first excitonic absorption peak. For 3 ML CdSe NPLs, the first excitonic absorption should be at wavelengths between 490 and 495 nm. For incomplete shifts, the exchange process is repeated. For a partial ligand exchange of the NPLs with varied thiolate/oleate coverage, smaller proportions of thiol are added and/or the reaction is stopped at different times between 2 min and 2 days by simple precipitation. After the completion of the ligand exchange, the NPLs are redispersed in 5 mL of toluene.

Ligand exchange (from carboxylates to halides): Adapted from ref[34] Similarly to the ligand exchange with thiols, a volume of NPLs solution equivalent to 0.08 mmol of cadmium, is precipitated and redispersed in 5 mL toluene and 500 µL OLA. To this mixture, the required volume of the $Cd(X)_2$ solution is added in order to have n_X (mol) : $n_{Cd(surface)}$ (mol) = 4 : 1. After reacting overnight under constant stirring, the product is washed with a mixture of toluene and methanol 2-3 times and redispersed in 5 mL of toluene.

Copper precursor for cation exchange: In a glovebox supplied with argon, 12 mg of $[Cu(CH_3CN)_4]PF_6$ is mixed with 400 µL anhydrous methanol and the mixture is stirred for 10 min. Once homogeneous, the solution is diluted with 3.6 mL of toluene.

Copper exchange on CdSe NPLs: For each population of NPLs, a volume of NPLs solution containing 0.016 mmol of total cadmium is precipitated and introduced in a glovebox under argon. All the following processes happened inside the glovebox. The precipitated NPLs are suspended again in 4 mL of toluene (anhydrous). The solution of copper precursor is injected into the solution of CdSe NPLs at a constant rate of 0.1 $mL.h^{-1}$. At the end of the injection, the dark suspension, corresponding to $Cu_{2-x}Se$, is left to stir for 10 min before being washed with a volume of 1:1 of toluene and methanol 3-4 times. The NPLs are redispersed in 1 mL toluene for further use. For kinetic studies of the copper exchange reaction, the copper precursor solution is injected at once. Aliquots are taken at different time and directly centrifuged to quench the reaction.

Transmission electron microscopy (TEM): A drop of diluted NPLs solution was drop-cast onto a copper grid covered with an amorphous carbon film. The grid was degassed overnight under secondary vacuum. Imaging was conducted using JEOL 2010 transmission electron microscope, operated at 200 kV. Complementarily, TEM/STEM observations were made on a Titan Themis 200 microscope (FEI/Thermo Fischer Scientific) equipped with a geometric aberration corrector on the probe. The microscope was also equipped with the ”Super-X” systems for EDX analysis with a detection angle of 0.9 steradian. The observations were made at 200 kV with a probe current of about 35 pA and a half-angle of convergence of 17 mrad. HAADF-STEM images were acquired with a camera length of 110 mm (inner/outer collection angles were respectively 69 and 200 mrad).

X-ray photoemission: High-resolution X-ray photoemission measurements were performed on the Tempo beamline at the synchrotron Soleil. Films of nanocrystals were spin-cast onto a Si substrate coated with 80 nm of Au. We select sample with short thiol to ensure that film gets conductive and prevent electrostatic charging of the film under X-ray beam. The samples were introduced in the preparation chamber and degassed under a vacuum below 10^{-9} mbar for at least two hours. Then the samples were introduced into the analysis chamber. The signal was acquired with a MBS A-1 photoelectron analyzer. The acquisition was done at a constant pass energy (50 eV) within the detector. A photon energy of 700 eV was used for the analysis of the core levels. The binding energy (BE) scale was calibrated using the gold substrate (Au $4f_{7/2}$ BE = 84.0 eV) For the XPS spectra decomposition a Shirley background was subtracted and pseudo-Voight function with 20% weighted Lorentzian contribution was used.

Energy dispersive X-ray (EDX) spectroscopy: Few drops of a highly concentrated solution of NPLs were drop-cast onto a Si wafer with a (100) crystallographic orientation of its surface. The wafer was attached on a conductive carbon tape. The Si wafer was purchased from Agar Scientific and has a thickness of 460-530 µm. The instrument used for the EDX analysis is an FEI Magellan scanning electron microscope, operated at 20 kV and 1.6 nA. The X-Ray analysis is made with an Oxford Probe.

Absorption spectroscopy: UV-visible absorption spectra were obtained by a Cary5000 spectrometer. The samples were measured in a cuvette by suspending the NPLs in hexane. For VIS-NIR measurements, the NPLs were suspended in TCE and placed in a HELMA QS 100-10-40 quartz cuvette.

RESULTS AND DISCUSSION

For the sake of illustration, we start by performing a copper cation exchange on 3 monolayer (ML) thick CdSe nanoplatelets (NPLs) adapting the procedure from the work of Wang Y. *et al.*[27] The NPLs present a cubic zinc blende crystal structure and the thickness in the [001] direction is made of 3 planes of selenium sandwiched by 4 planes of cadmium.[4] On their surface, carboxylate ligands (mix of oleate (OA) and acetate (Ac)) ensure the neutrality of the particle as well as their colloidal stability in non-polar solvents. These

native ligands also induce an in-plane surface stress on the NPLs, such that they fold as helices or twists depending on their lateral dimensions,[33,35–37] as revealed by transmission electron microscopy (TEM) (**Figure 1**a). A copper cation exchange is here conducted by exposing the CdSe NPLs suspended in toluene to a copper precursor[15] (tetrakis(acetonitrile)copper(I) hexafluorophosphate, $[Cu(CH_3CN)_4]PF_6$) dissolved in methanol, which can be added at different rates (either dropwise or straight for kinetic studies). The cation exchange is driven by the higher solvation energy of Cd^{2+} compared to Cu^{+} in methanol and the stronger affinity of Cu^{+} with Se^{2-}. These two parameters help for the exit of Cd^{2+} from the CdSe NPLs and the formation of the $Cu_{2-x}Se$ nanoparticles.[19] Here, the obtained particles (**Figure 1**b) present a disordered appearance with poorly defined dimensionalities. Some areas get clearly aggregated which suggests a strong material reconstruction from a 2D initial aspect towards a bulkier material. To reveal the importance of the capping ligands during this procedure, we have exchanged the native carboxylates for halides (Supp Info Figure S1-2) and thiolates (**Figure 1**c-d). The iodide ligands, in particular, relieve the ligand-induced strain[34] and unfold the NPLs (Supp Info Figure S2). However, for both bromide and iodide the quality of the material obtained after cation exchange, is not satisfying and the 2D shape is mostly lost. The case of thiolates (RS^- with R an aliphatic chain) appears more interesting since the 2D shape is preserved after both the ligand exchange (**Figure 1**c, after which particles still roll-up) and the cation exchange (**Figure 1**d). Although folding may have been considered as a source of surface reorganization, whether to conduct the exchange on a flat surface (I^- capping) or not (RS^- capping) does not appear to be a criterion for maintaining the final 2D aspect. It is important to point out that the aggregation observed when using unsuitable ligands is irreversible and conducting a ligand exchange after the cation exchange does not allow recovering the initial 2D shape (Supp Info Figure S3).

With thiolate ligands, final $Cu_{2-x}Se$ particles present a flat 2D aspect. The stoichiometry of the particle determined by energy dispersive X-ray spectrometry (EDX) reveals a Cu:Se:S ratio of 7:3:1.8 compared to a theoretical ratio of 8:3:2. In the theoretical ratio the excess of chalcogens arises from the thiolate ligands that bring only one negative charge instead of 2 for the Se^{2-}. The experimental ratio reveals an understoichiometry of S which might come from a desorption of thiolate ligands or more precisely Cu-thiolate from the surface. Finally, the understoichiometry of Cu is estimated to ~ 10%, a value in agreement with the $Cu_{1.8}Se$ berzelianite structure. In the following the material will be called $Cu_{2-x}Se$. The absorption spectrum (**Figure 2**a) acquired over both the infrared and visible range reveals an exciton-featureless spectrum. It first reveals that CdSe is fully transformed. Such spectrum is consistent with the one from a plasmonic material as expected from under-stoichiometric $Cu_{2-x}Se$.[38] In the infrared, the feature relative to the C-H bond (at 2900 cm^{-1}) is the main observed feature. Only traces from C=O (from oleic acid at 1552 cm^{-1}) and S-H at around 730 cm^{-1} can be noticed.

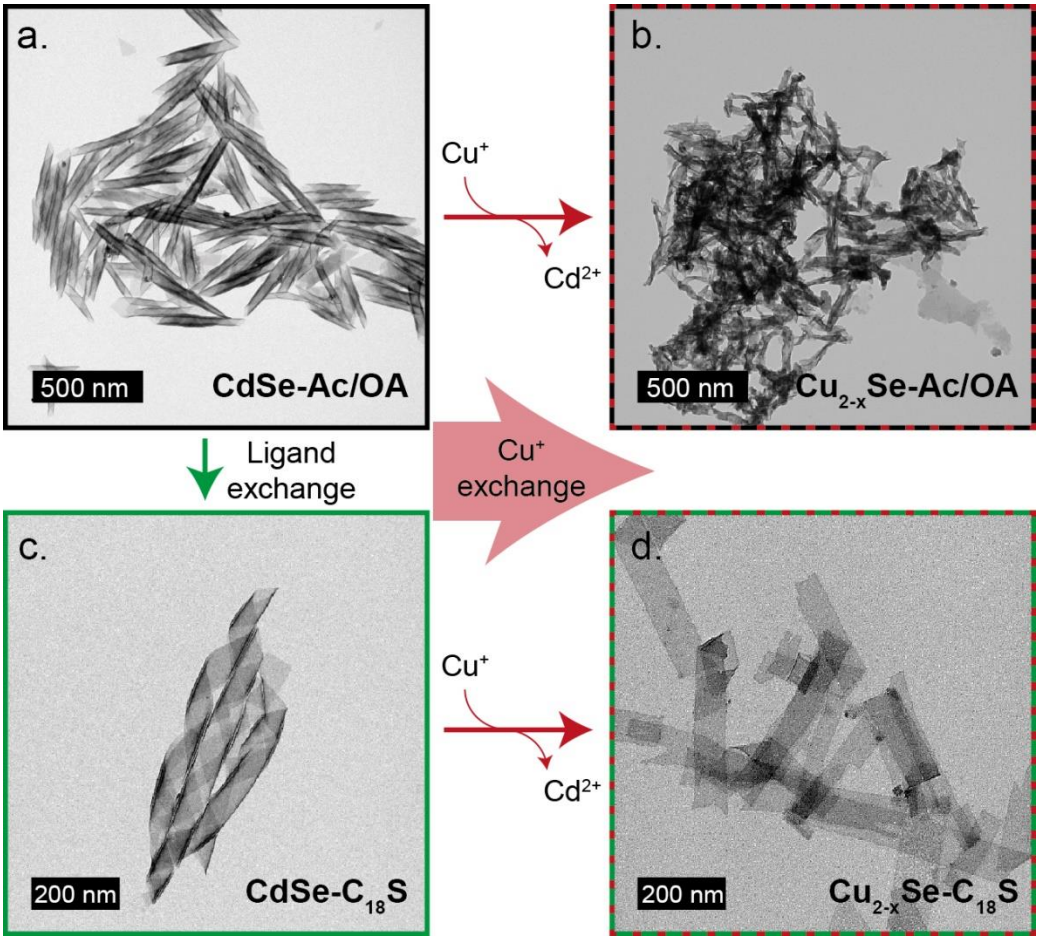

Figure 1 Effect of capping ligands on the final morphology of the particles during the cation exchange procedure on 2D NPLs*. a. TEM image of 3 ML CdSe NPLs capped with native carboxylate ligands (Ac/OA). b. TEM image of $Cu_{2-x}Se$ NPLs obtained after treating CdSe NPLs in Figure 1a with Cu^+. c. TEM image of 3 ML CdSe NPLs obtained after ligand exchange (from oleate to octadecanethiolate noted $C_{18}S$)) on NPLs in Figure 1a. d. TEM image of the $Cu_{2-x}Se$ NPLs obtained after treating CdSe NPLs in Figure 1c with Cu^+.*

X-ray photoemission is then used as a more surface sensitive method (**Figure 2**b-d). The survey spectrum (**Figure 2**b) confirms the absence of Cd (binding energy of 405 eV), and thus the full exchange of the initial CdSe NPLs, as already suggested by absorption and EDX. For thiolate capped $Cu_{2-x}Se$ NPLs, features from Cu, S and Se are observed. We also notice the presence of carbon and oxygen that result from thiolate ligands and from the leftovers native carboxylate ligands. The Cu 3p state (**Figure 2**c) exhibits three contributions.[39] The primary contribution, denoted peak 1 (~ 78%), appears at a binding energy of ≈75 eV and can be confidently attributed to Cu^+ bonded to chalcogenides. The contribution appearing at higher binding energy (77.8 eV), denoted peak 2 (~ 14%), is certainly associated to Cu^{2+}, which comes from the oxidation of Cu^+. Finally, the lowest binding energy contribution, denoted peak 3 with a low weight (~ 8%), may result from the formation of metallic copper traces. The two main contributions (i.e. peaks 1 and 2) may have been attributed to two types of Cu^+ bound to the two types of chalcogenides (i.e. selenium and sulfur). Those bound to selenium, whose electronegativity is lower than that of sulfur, should present a reduced binding energy (i.e. peak 2). Those linked to sulfur should have a higher binding energy (i.e. peak 1). However this situation is not compatible with the stoichiometry of $Cu_{2-x}Se$-thiolate NPLs in which most of Cu^+ bound to selenide and hence which binding energy intensity should be the highest. The peak relative to the Se 3d states reveals a more complex environment, with several contributions (**Figure 2**d). However, all of them present a limited binding energy in the 53-55 eV range compatible with a reduced form of selenium (*i.e.* Se^{2-}),[40] also note that the absence of high binding energy contribution (i.e. above 58 eV) excludes the formation of selenium oxide.

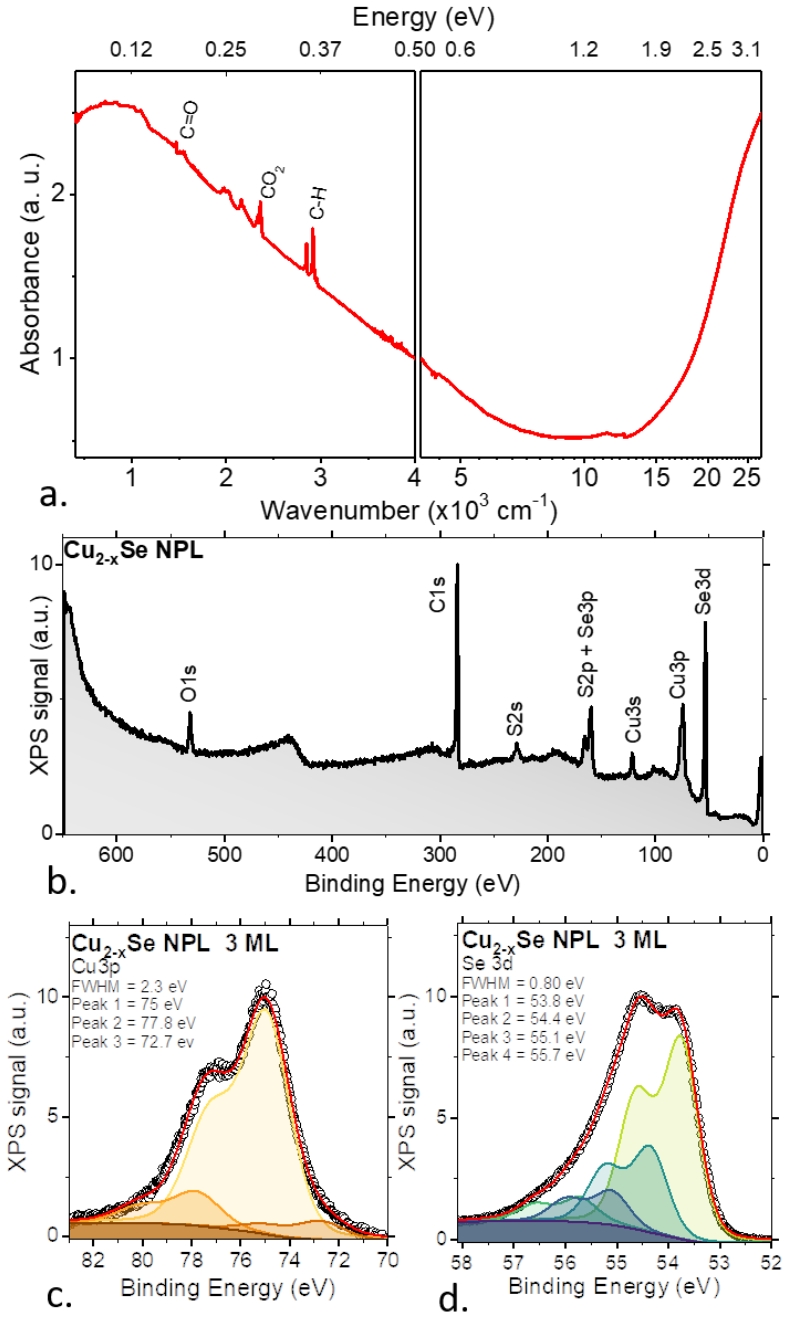

Figure 2 Surface chemistry analysis of the $Cu_{2-x}Se$ NPLs capped with ethanethiolates. *a. Infrared and visible absorption spectrum for Cu_2Se NPLs capped with thiolates. b. X-ray photoemission survey spectrum. c. X-ray photoemission spectrum for the Cu 3p states. d. X-ray photoemission spectrum for the Se 3d states.*

After cation exchange, the overall shape of NPLs remains preserved. However, since it is an aliovalent cation exchange, the crystal structure is modified. If the anion sublattice is preserved over the cation exchange, it might be expected to obtain nanoparticles with a cubic crystal structure. Thus $Cu_{2-x}Se$ NPLs should present a berzellianite crystal structure with a lattice parameter of $a_{Cu2-xSe}$ = 0.576 nm.[27] Indeed the X-ray diffraction patterns of CdSe NPLs and $Cu_{2-x}Se$ NPLs present the same series of peaks from a cubic phase relative to the families of planes (111), (200), (220) and (311) (**Figure 3**). Due to the smaller lattice parameter of $Cu_{2-x}Se$[27] compared to CdSe (a_{CdSe} = 0.608 nm),[4] the diffraction peaks appear shifted toward higher angles. Indeed, the Cu-Se bond, being shorther than Cd-Se bond, induces a lattice shrinkage. It is well established that $Cu_{2-x}Se$ (for x between 0 and 0.5) present multiple polymorphs, however after further comparisons with tetragonal, monoclinic, or orthorhombic crystal structures, the berzelianite crystal

structure remains the most likely (see Supp Info Figure S4).[29] This observation is further confirmed with selected area electron diffraction (SAED) image performed on $Cu_{2-x}Se$ NPLs from 4 ML CdSe NPLs, which shows rings (with spots) at positions in agreement with the cubic phases (see Supp Info Figure S5). Thus the anionic sublattice seems to be preserved over the cation exchange and remains cubic.[21] To understand the benefit of thiolates in maintaining the 2D shape, it is worth mentioning that thiolates ligands induce an in-plane compressive stress of the CdSe lattice in the NPLs (as evidenced by the shift toward high angles of the (220) peak) contrary to the native carboxylate ligands which were inducing tensile in-plane stress to the same CdSe NPLs.[33,36] This pre-contraction of the lattice in presence of thiolates should minimize the lattice reorganization as the cations get replaced.

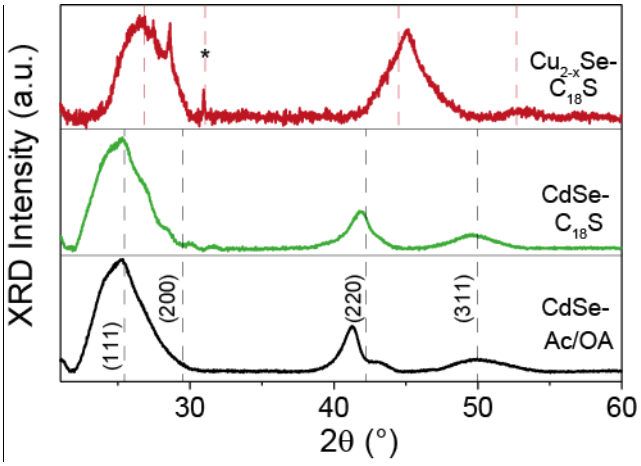

Figure 3 Structure of CdSe and $Cu_{2-x}Se$ NPLs*. a. X-ray diffractograms for 3 ML CdSe NPLs capped with carboxylates (black curve), and octadecanethiolates (green curve), and for $Cu_{2-x}Se$ NPLs after cation exchange capped with octadecanethiolates (red curve). The stat symbol (*) highlights the peak arising from the Si substrate.The dash lines in black and red represent the position of the peaks for a cubic cell of lattice parameter of 0.608 nm (CdSe) and 0.576 nm ($Cu_{2-x}Se$ berzelinate)*

We have then explored how the thiolate chain length impacts the dynamics of the cation exchange. We graft on the surface of the CdSe NPLs, thiolates with aliphatic chains ranging from 4 to 18 carbons ($C_nH_{2n+1}S^-$ for n=4, 8, 12 and 18 noted hereafter C_nS) (Supp Info Figure S6). We then track the Cd content during the cation exchange as a function of time using EDX. To stop the reaction, aliquots from the reaction mixture are precipitated and redispersed in fresh solvent (*i.e.* not containing Cu^+ precursor). Hence, an error range of ±1min is applied to take into account the sampling and precipitating steps and the experimental error. TEM images of particles after the full cation exchange reveal that all four thiolate ligands enable to maintain the 2D shape of NPLs (**Figure 4**c-f). It shows that the benefit of thiolate ligands arises from the anchoring group rather than from the aliphatic chain and its length. The anchoring group of all thiolate ligands applies a similar stress on the CdSe NPLs, which minimizes surface reconstruction induced by the cation exchange. However, the chain length of the thiolate ligands does impact the final particle's folding. A shorter chain leads to a more bent particle, while a longer one results in an almost flat structure. These results are similar to those observed on CdSe.[35,36] Beyond the folding, the ligand length also drives the exchange kinetics (**Figure 4**a-b). The overall trend is that shorter thiolates lead to a faster exchange. Since all thiolate ligands tested enable to preserve the 2D shape, we conclude that surface reconstruction is not primarily driven by kinetic (*i.e.,* how fast the anion lattice may be destabilized) but rather by thermodynamic considerations (*i.e.,* differences in lattice parameter and applied strain).

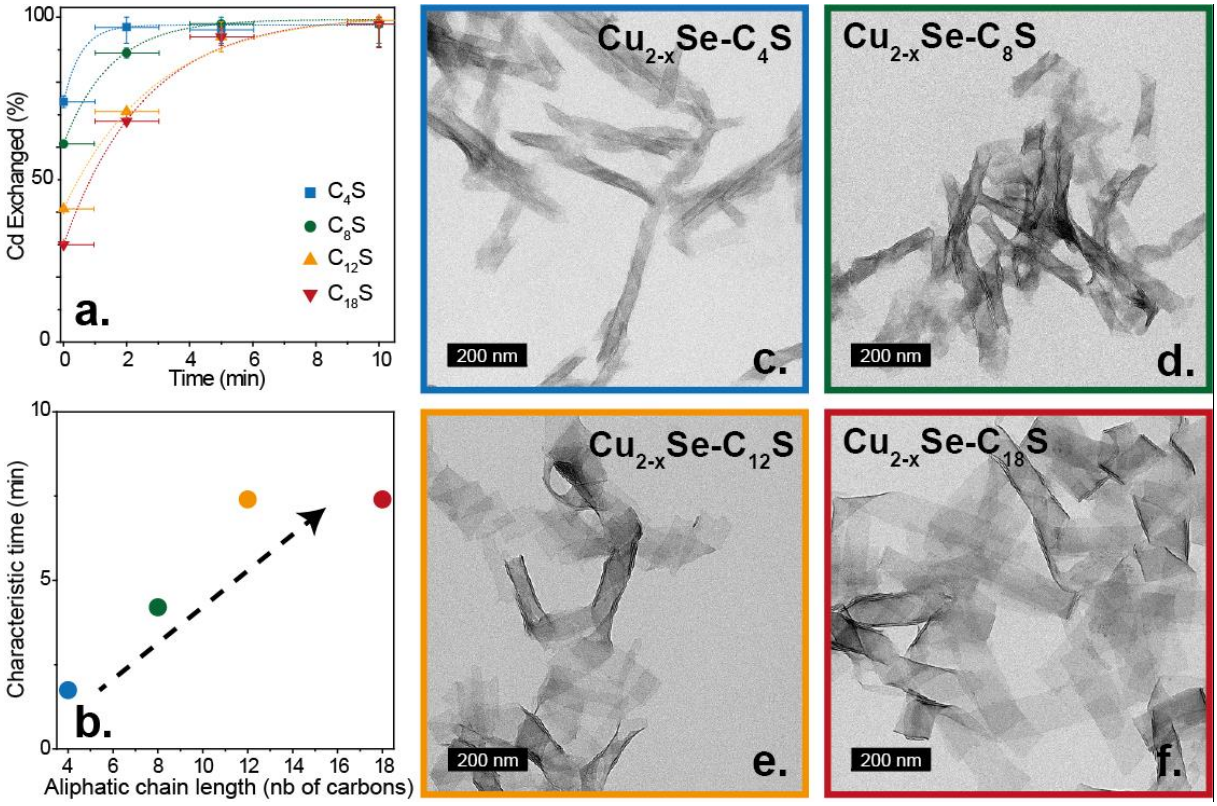

Figure 4 Impact of ligand length on cation exchange*. a. Ratio of Cd exchanged tracked by EDX as a function of time during the Cu cation exchange conducted on 3 ML CdSe NPLs capped with $C_nH_{2n+1}S$-thiolate ligands for n= 4, 8, 12 and 18 notes C_nS. b. Characteristic duration for the cation exchange (obtained by fitting data of Figure 4a. using a single exponential) as a function of the thiolate aliphatic chain length. c-f. TEM images of the obtained $Cu_{2-x}Se$ NPLs capped with thiolates of various aliphatic chain lengths. TEM images of the initial CdSe NPL capped with the same thiols are given in Supp Info Figure S6.*

While the thiolate aliphatic chain length is not critical to maintain the 2D shape, the overall surface coverage appears to be (**Figure 5**). We have shown that CdSe NPLs only covered by carboxylates couldn't maintain their 2D shape during cation exchange while when they are capped with thiolates the initial shape is maintained. We have then explored intermediate steps. To do so, we conducted the ligand exchange towards octadecanethiolates and stopped it before its completion (*i.e.*, the solution is precipitated). The thiolate coverage can be followed with EDX spectroscopy while measuring the sulfur to cadmium ratio in the sample. The CdSe NPLs capped with a mixture of carboxylates and thiolates are then redispersed, and further submitted to a cation exchange procedure. As for the ligand length study, we track the exchange by monitoring the Cd content using EDX. We observed a lengthening of the cation exchange time with the thiolate coverage, while most of ligands (oleate and octadecanethiolate) both present a C_{18} alkyl chain. Thus, the kinetics is not only driven by the ligand length. We speculate that the stronger binding of thiolates, with respect to carboxylates, to a soft metal, slows down the release of the native cadmium.

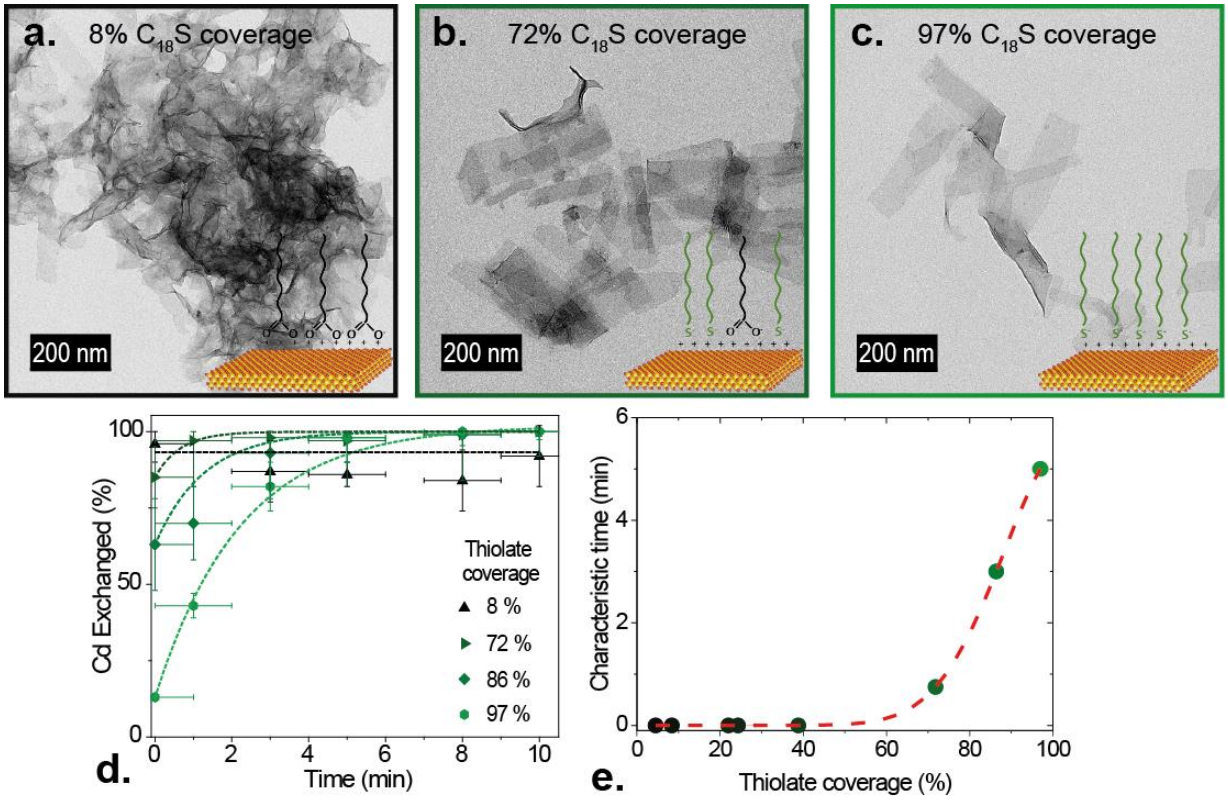

Figure 5 Impact of the thiol coverage*. a-c. TEM images of $Cu_{2-x}Se$ particles obtained after cation exchange on 3 ML CdSe NPLs, while the exchange is conducted with various octadecanethiolate ($C_{18}S$) coverages. The inset schematizes the particle and the various associated surface chemistries, ranging from pure carboxylates to pure octadecanethiolates. TEM images of the initial CdSe NPLs are given in Supp Info Figure S7. d. Ratio of Cd exchanged tracked with EDX as a function of time during the Cu^+ cation exchange conducted on CdSe NPLs capped with different octadecanethiolates coverages. e. Characteristic duration for the cation exchange (obtained by fitting data in Figure 5d, using a single exponential) as a function of octadecanethiolates coverages.*

Given the 2D shape of the nanoparticles, it is reasonable to ask which facets are involved during the cation exchange. Indeed, it can be the wide top and bottom facets, the narrow side facets or both combined. To answer, this question, we have prepared 4 ML CdSe NPLs capped with $C_{18}S$ that we only partially exchanged with Cu^+ by reducing the amount of added Cu^+ precursor. The Figure 6a (Supp Info Figure S8) shows the High Angle Annular Dark Field – Scanning Transmission Electron Microscopy (HAADF-STEM) image of these NPLs lying flat on the substrate (lying on their edges). The Figure 6b-d represent the corresponding X-ray mapping and show greater exchange at the periphery of NPLs than in the core, inducing the formation of core/crown NPLs. Thus, it appears that exchange preferentially takes place via the side facets, where ligand density is lower than on the wide facets.[41] Such heterostructures have already been observed with nanorods where cation exchange with Cu^+ happens first through the tips.[42] But concerning NPLs, these results seem to contradict those reported on thick core/shell NPLs where the exchange happened through the wide facets[28]. However, the main difference is the surface chemistry. Here, the strong electrostatic interaction between the thiolates and the surface Cd may impose an additional barrier to wide facets, which is all the more difficult to overcome as the aliphatic chains are long. Indeed, although cation exchange takes place mainly at the edges, we can't rule out the possibility that exchange also takes place on the wide facets for shorter ligands.[43–45]We can also note that, in these core/crown $Cu_{2-x}Se$/CdSe NPLs, the edges are a bit damaged while in purely exchanged $Cu_{2-x}Se$ NPLs (-Figure 6 e-h), it is not the case. The interface between $Cu_{2-x}Se$ and CdSe might be fragile due to the thin NPLs. Besides, there might be a reorganization of Cu^+ and Cd^{2+} leading to a segregation of phases in the NPLs and thus a weakening of the interface.

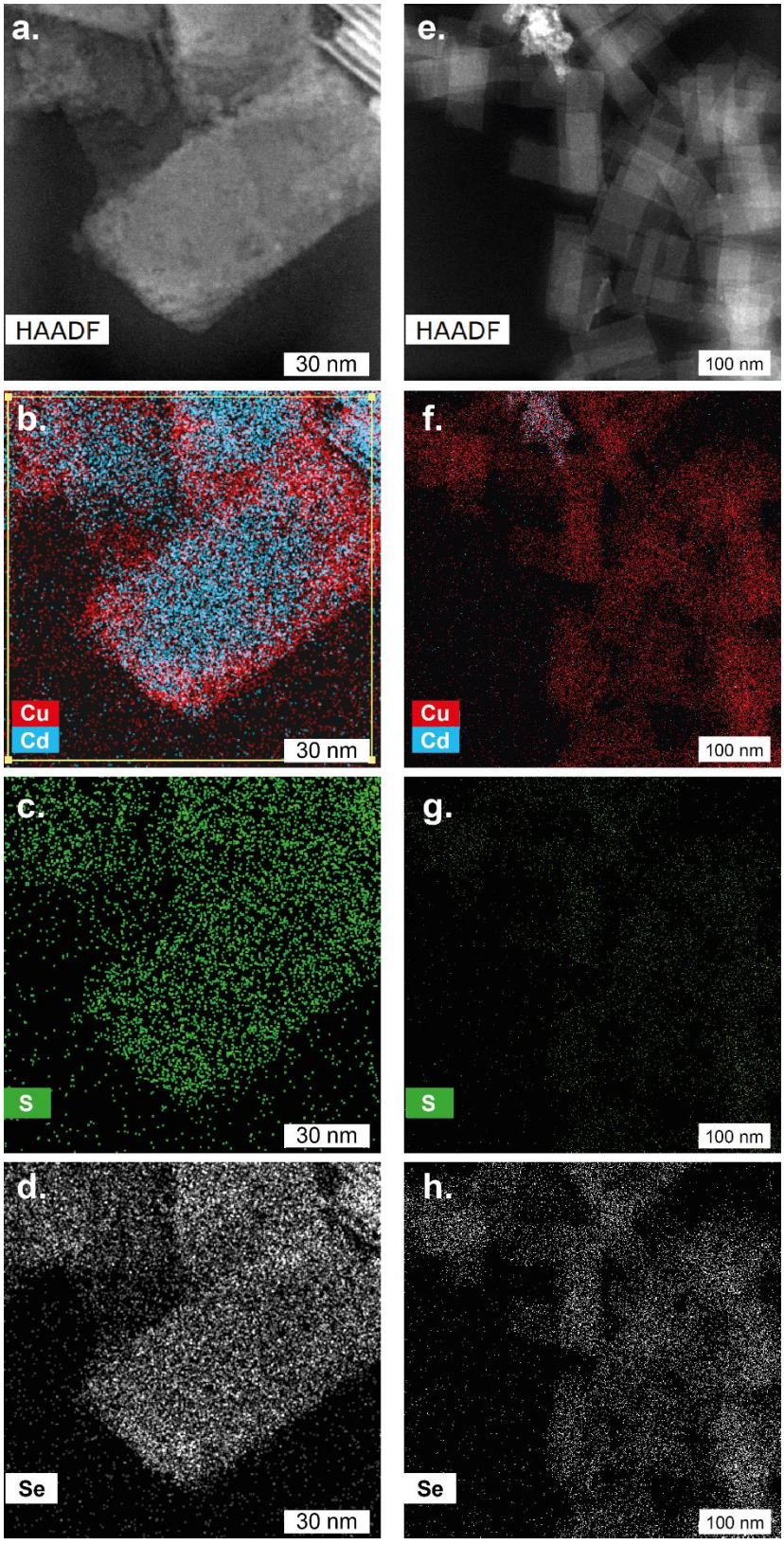

Figure 6 : High Angle Annular Dark Field – Scanning Transmission Electron Microscopy images of (a) partially exchanged 4 ML CdSe-C_{18}S NPLs with Cu^+ and (b) Cu_{2-x}Se-C_{18}S NPLs with corresponding Energy Dispersive X-ray Spectroscopy (b) and (f) Cu and Cd maps (c) and (g) S maps and (d) and (h) Se map.

To finish, we have tested the versatility of the results by conducting the cation exchange on CdSe NPLs with various thicknesses (ranging from 2 to 5 MLs, see **Figure 7**) and to another composition (CdS NPLs, Supp Info Figure S9). Thiolate capping is compatible in all cases with preservation of the initial shape, while their lateral extension can be quite different. Besides, it is interesting to note that 2 ML CdSe NPLs capped with thiolates present as many atomic planes as 3 ML CdSe NPLs capped with carboxylates (4 anionic planes and 3 cationic planes for 2 ML CdSe-C_{18}S vs 4 cationic planes and 3 anionic planes for 3 ML CdSe-

Ac/OA). So, it is indeed the effect of ligands and not the thickness, that preserves the 2D shape of nanoparticles during cation exchange. In CdS NPLs, we observe a similar dramatic shape reconstruction with oleates, while thiolates also preserve the shape after cation exchange with Cu^{+}. A back exchange from Cu^{+} to Cd^{2+} has been further tested on $Cu_{2-x}Se$ NPLs capped with thiolate (Supp Info Figure S10) and despite the optical properties after back exchange not being as well-defined as the initial ones, the average positions of the excitonic features are in agreement with the native NPLs. It thus shows that the $Cu_{2-x}Se$ NPLs capped with thiolate ligands preserve not only the 2D shape but also a thickness with a roughness in the order of an atomic monolayer.

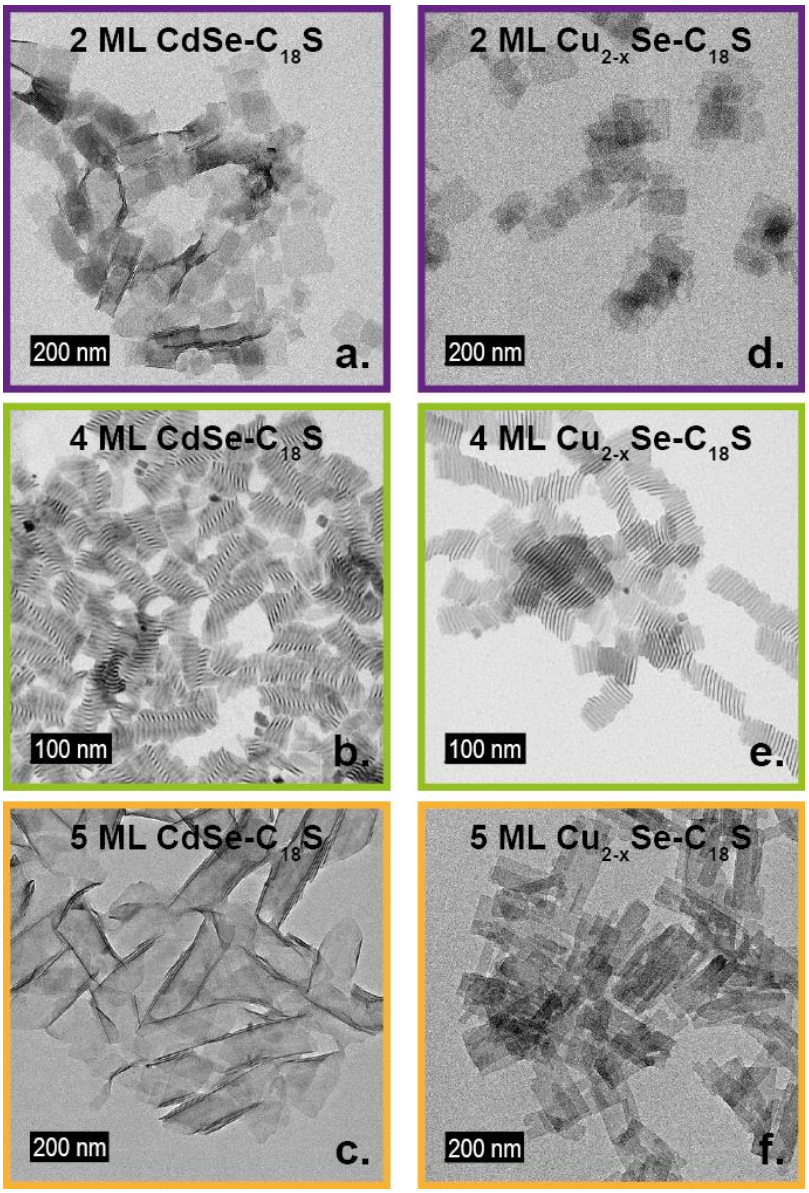

Figure 7 Application to other thicknesses*. a, b and c are respectively TEM images of 2 ML, 4 ML, and 5 ML CdSe NPLs capped with octadecanethiolates, d, e and f are respectively TEM images of the $Cu_{2-x}Se$ NPLs obtained from respectively a, b and c.*

CONCLUSION

To summarize, we have presented evidence that surface chemistry plays a critical role in the kinetics and thermodynamics of the cation exchange process. To prevent surface reconstruction in 2D NPLs, the ligands need to exert pressure on the lattice, minimizing the lattice distortion during the cation exchange. Conversely, parameters such as the ligand length, ligand binding energy or the flatness of the material when the cation exchange reaction is conducted, do affect the speed of reaction and less the shape

reconstruction. We finally emphasize that thiolates appear to be an effective ligand to maintain the shape of NPLs of various thicknesses and compositions during the cadmium-to-copper exchange.

SUPPORTING INFORMATION

Figures S1-S3 present the effect of ligands on the final morphology of NPLs after cation exchange with Cu^+. Figures S4-S5 present the diffraction of $Cu_{2-x}Se$ NPLs. Figures S6-S7 present the optical properties and TEM images of NPLs capped with different thiolate ligands and in different proportions related to carboxylate native ligands. Figure S8 shows STEM images of partially exchanged NPLs. Figure S9 presents TEM images of $Cu_{2-x}S$ NPLs obtained from CdSe NPLs. Figure S10 presents the optical properties and TEM images of NPLs after cations exchange with Cu^+ and back-exchange with Cd^{2+}.

ACKNOWLEDEGMENTS

The project is supported by ERC grants Ne2deM (grant 853049), blackQD (grant n° 756225) and AQDtive (grant n°101086358). This work is supported by French state funds managed by the ANR with grants: Copin (ANR-19-CE24-0022), Frontal (ANR-19-CE09-0017), Graskop (ANR-19-CE09-0026), NITQuantum (ANR-20-ASTR-0008), Bright (ANR-21-CE24-0012), MixDFerro (ANR-21-CE09-0029.) and Quicktera (ANR-22-CE09-0018).

CONFLICT OF INTEREST

The authors declare no competing financial interest.

REFERENCES

(1) Erdem, T.; Demir, H. V. Color Science of Nanocrystal Quantum Dots for Lighting and Displays. *Nanophotonics* **2013**, *2*, 57–81.

(2) Weidman, M. C.; Beck, M. E.; Hoffman, R. S.; Prins, F.; Tisdale, W. A. Monodisperse, Air-Stable PbS Nanocrystals *via* Precursor Stoichiometry Control. *ACS Nano* **2014**, *8*, 6363–6371.

(3) Cademartiri, L.; Bertolotti, J.; Sapienza, R.; Wiersma, D. S.; von Freymann, G.; Ozin, G. A. Multigram Scale, Solventless, and Diffusion-Controlled Route to Highly Monodisperse PbS Nanocrystals. *J Phys Chem B* **2006**, *110*, 671–673.

(4) Diroll, B. T.; Guzelturk, B.; Po, H.; Dabard, C.; Fu, N.; Makke, L.; Lhuillier, E.; Ithurria, S. 2D II–VI Semiconductor Nanoplatelets: From Material Synthesis to Optoelectronic Integration. *Chem Rev* **2023**, *123*, 3543–3624.

(5) Khan, A. H.; Brescia, R.; Polovitsyn, A.; Angeloni, I.; Martín-García, B.; Moreels, I. Near-Infrared Emitting Colloidal PbS Nanoplatelets: Lateral Size Control and Optical Spectroscopy. *Chemistry of Materials* **2017**, *29*, 2883–2889.

(6) Sonntag, L.; Shamraienko, V.; Fan, X.; Samadi Khoshkhoo, M.; Kneppe, D.; Koitzsch, A.; Gemming, T.; Hiekel, K.; Leo, K.; Lesnyak, V.; Eychmüller, A. Colloidal PbS Nanoplatelets Synthesized *via* Cation Exchange for Electronic Applications. *Nanoscale* **2019**, *11*, 19370–19379.

(7) Manteiga Vázquez, F.; Yu, Q.; Klepzig, L. F.; Siebbeles, L. D. A.; Crisp, R. W.; Lauth, J. Probing Excitons in Ultrathin PbS Nanoplatelets with Enhanced Near-Infrared Emission. *J Phys Chem Lett* **2021**, *12*, 680–685.

(8) Bhandari, G. B.; Subedi, K.; He, Y.; Jiang, Z.; Leopold, M.; Reilly, N.; Lu, H. P.; Zayak, A. T.; Sun, L. Thickness-Controlled Synthesis of Colloidal PbS Nanosheets and Their Thickness-Dependent Energy Gaps. *Chemistry of Materials* **2014**, *26*, 5433–5436.

(9) Klepzig, L. F.; Leon Biesterfeld, ab; Michel Romain, ab; Niebur, A.; Anja Schlosser, ab; Jens, ac H.; cd, ubner; Lauth, J. Colloidal 2D PbSe Nanoplatelets with Efficient Emission Reaching the Telecom O-, E-and S-Band †. *Nanoscale Adv.* **2022**, *4*, 590–599.

(10) Dabard, C.; Planelles, J.; Po, H.; Izquierdo, E.; Makke, L.; Gréboval, C.; Moghaddam, N.; Khalili, A.; Dang, T. H.; Chu, A.; Pierini, S.; Abadie, C.; Cavallo, M.; Bossavit, E.; Xu, X. Z.; Hollander, P.; Silly, M.; Lhuillier, E.; Climente, J. I.; Ithurria, S. Optimized Cation Exchange for Mercury Chalcogenide 2D Nanoplatelets and Its Application for Alloys. *Chemistry of Materials* **2021**, *33*, 9252–9261.

(11) Izquierdo, E.; Robin, A.; Keuleyan, S.; Lequeux, N.; Lhuillier, E.; Ithurria, S. Strongly Confined HgTe 2D Nanoplatelets as Narrow Near-Infrared Emitters. *J Am Chem Soc* **2016**, *138*, 10496–10501.

(12) Livache, C.; Izquierdo, E.; Martinez, B.; Dufour, M.; Pierucci, D.; Keuleyan, S.; Cruguel, H.; Becerra, L.; Fave, J. L.; Aubin, H.; Ouerghi, A.; Lacaze, E.; Silly, M. G.; Dubertret, B.; Ithurria, S.; Lhuillier, E. Charge Dynamics and Optolectronic Properties in HgTe Colloidal Quantum Wells. *Nano Lett* **2017**, *17*, 4067–4074.

(13) Salzmann, B. B. V; De Wit, J.; Li, C.; Arenas-Esteban, D.; Bals, S.; Meijerink, A.; Vanmaekelbergh, D. Two-Dimensional CdSe-PbSe Heterostructures and PbSe Nanoplatelets: Formation, Atomic Structure, and Optical Properties. *J. Phys. Chem. C* **2022**, *126*, 1513–1522.

(14) Galle, T.; Samadi Khoshkhoo, M.; Martin-Garcia, B.; Meerbach, C.; Sayevich, V.; Koitzsch, A.; Lesnyak, V.; Eychmüller, A. Colloidal PbSe Nanoplatelets of Varied Thickness with Tunable Optical Properties. *Chemistry of Materials* **2019**, *31*, 3803–3811.

(15) Son, D. H.; Hughes, S. M.; Yin, Y.; Paul Alivisatos, A. Cation Exchange Reactions in Ionic Nanocrystals. *Science (1979)* **2004**, *306*, 1009–1012.

(16) Li, H.; Brescia, R.; Krahne, R.; Bertoni, G.; Alcocer, M. J. P.; D'Andrea, C.; Scotognella, F.; Tassone, F.; Zanella, M.; De Giorgi, M.; Manna, L. Blue-UV-Emitting ZnSe(Dot)/ZnS(Rod) Core/Shell Nanocrystals Prepared from CdSe/CdS Nanocrystals by Sequential Cation Exchange. *ACS Nano* **2012**, *6*, 1637–1647.

(17) Van Der Stam, W.; Bladt, E.; Rabouw, F. T.; Bals, S.; De Mello Donega, C. Near-Infrared Emitting CuInSe 2 / CuInS 2 Dot Core/Rod Shell Heteronanorods by Sequential Cation Exchange. *ACS Nano* **2023**, *9*, 11430–11438.

(18) Lesnyak, V.; George, C.; Genovese, A.; Prato, M.; Casu, A.; Ayyappan, S.; Scarpellini, A.; Manna, L. Alloyed Copper Chalcogenide Nanoplatelets via Partial Cation Exchange Reactions. *ACS Nano* **2014**, *8*, 8407–8418.

(19) De Trizio, L.; Manna, L. Forging Colloidal Nanostructures via Cation Exchange Reactions. *Chem Rev* **2016**, *116*, 10852–10887.

(20) Beberwyck, B. J.; Surendranath, Y.; Alivisatos, A. P. Cation Exchange: A Versatile Tool for Nanomaterials Synthesis. *Journal of Physical Chemistry C* **2013**, *117*, 19759–19770.

(21) Fenton, J. L.; Steimle, B. C.; Schaak, R. E. Structure-Selective Synthesis of Wurtzite and Zincblende ZnS, CdS, and CuInS 2 Using Nanoparticle Cation Exchange Reactions. *Inorg Chem* **2019**, *58*, 672–678.

(22) Li, H.; Zanella, M.; Genovese, A.; Povia, M.; Falqui, A.; Giannini, C.; Manna, L. Sequential Cation Exchange in Nanocrystals: Preservation of Crystal Phase and Formation of Metastable Phases. *Nano Lett* **2011**, *11*, 4964–4970.

(23) De Trizio, L.; Gaspari, R.; Bertoni, G.; Kriegel, I.; Moretti, L.; Scotognella, F.; Maserati, L.; Zhang, Y.; Messina, G. C.; Prato, M.; Marras, S.; Cavalli, A.; Manna, L. Cu 3-x P Nanocrystals as a Material Platform for Near-Infrared Plasmonics and Cation Exchange Reactions. *Chem. Mater.* **2015**, *27*, 1120–1128.

(24) Shan, X.; Zhou, Y.; Li, B.; Zeng, Z.; Ji, B. Wurtzite InAs Nanocrystals with Short-Wavelength Infrared Emission Synthesized through the Cation Exchange of Cu 3 As Nanocrystals. *Chem. Mater* **2023**, *35*, 2569–2578.

(25) Gréboval, C.; Izquierdo, E.; Livache, C.; Martinez, B.; Dufour, M.; Goubet, N.; Moghaddam, N.; Qu, J.; Chu, A.; Ramade, J.; Aubin, H.; Cruguel, H.; Silly, M.; Lhuillier, E.; Ithurria, S. Impact of Dimensionality and Confinement on the Electronic Properties of Mercury Chalcogenide Nanocrystals. *Nanoscale* **2019**, *11*, 3905–3915.

(26) Sokolova, A. V.; Skurlov, I. D.; Babaev, A. A.; Perfenov, P. S.; Miropoltsev, M. A.; Danilov, D. V.; Baranov, M. A.; Kolesnikov, I. E.; Koroleva, A. V.; Zhizhin, E. V.; Litvin, A. P.; Fedorov, A. V.; Cherevkov, S. A. Near-Infrared Emission of HgTe Nanoplatelets Tuned by Pb-Doping. *Nanomaterials* **2022**, *12*, 4198.

(27) Wang, Y.; Zhukovskyi, M.; Tongying, P.; Tian, Y.; Kuno, M. Synthesis of Ultrathin and Thickness-Controlled Cu $_{2-x}$Se Nanosheets via Cation Exchange. *J Phys Chem Lett* **2014**, *5*, 3608–3613.

(28) Bouet, C.; Laufer, D.; Mahler, B.; Nadal, B.; Heuclin, H.; Pedetti, S.; Patriarche, G.; Dubertret, B. Synthesis of Zinc and Lead Chalcogenide Core and Core/Shell Nanoplatelets Using Sequential Cation Exchange Reactions. *Chemistry of Materials* **2014**, *26*, 3002–3008.

(29) Berends, A. C.; Van Der Stam, W.; Akkerman, Q. A.; Meeldijk, J. D.; Van Der Lit, J.; De Mello Donega, C. Anisotropic 2D Cu 2−x Se Nanocrystals from Dodecaneselenol and Their Conversion to CdSe and CuInSe 2 Nanoparticles. *Chem. Mater* **2018**, *30*, 3836–3846.

(30) Justo, Y.; Sagar, L. K.; Flamee, S.; Zhao, Q.; Vantomme, A.; Hens, Z. Less Is More. Cation Exchange and the Chemistry of the Nanocrystal Surface. *ACS Nano* **2014**, *8*, 7948–7957.

(31) Fan, Z.; Lin, L. C.; Buijs, W.; Vlugt, T. J. H.; Van Huis, M. A. Atomistic Understanding of Cation Exchange in PbS Nanocrystals Using Simulations with Pseudoligands. *Nat Commun* **2016**, *7*, 11503.

(32) Shamraienko, V.; Spittel, D.; Hübner, R.; Samadi Khoshkhoo, M.; Weiß, N.; Georgi, M.; Borchert, K. B. L.; Schwarz, D.; Lesnyak, V.; Eychmüller, A. Cation Exchange on Colloidal Copper Selenide Nanosheets: A Route to Two-Dimensional Metal Selenide Nanomaterials. *J Mater Chem C Mater* **2021**, *9*, 16523–16535.

(33) Antanovich, A.; Achtstein, A. W.; Matsukovich, A.; Prudnikau, A.; Bhaskar, P.; Gurin, V.; Molinari, M.; Artemyev, M. A Strain-Induced Exciton Transition Energy Shift in CdSe Nanoplatelets: The Impact of an Organic Ligand Shell. *Nanoscale* **2017**, *9*, 18042–18053.

(34) Dufour, M.; Qu, J.; Greboval, C.; Méthivier, C.; Lhuillier, E.; Ithurria, S. Halide Ligands to Release Strain in Cadmium Chalcogenide Nanoplatelets and Achieve High Brightness. *ACS Nano* **2019**, *13*, 5326–5334.

(35) Martinet, Q.; Baronnier, J.; Girard, A.; Albaret, T.; Saviot, L.; Mermet, A.; Abecassis, B.; Margueritat, J.; Mahler, B. Ligand-Dependent Nano-Mechanical Properties of CdSe Nanoplatelets: Calibrating Nanobalances for Ligand Affinity Monitoring. *Nanoscale* **2021**, *13*, 8639–8647.

(36) Po, H.; Dabard, C.; Roman, B.; Reyssat, E.; Bico, J.; Baptiste, B.; Lhuillier, E.; Ithurria, S. Chiral Helices Formation by Self-Assembled Molecules on Semiconductor Flexible Substrates. *ACS Nano* **2022**, *16*, 2901–2909.

(37) Bouet, C.; Tessier, M. D.; Ithurria, S.; Mahler, B.; Nadal, B.; Dubertret, B. Flat Colloidal Semiconductor Nanoplatelets. *Chemistry of Materials* **2013**, *25*, 1262–1271.

(38) Luther, J. M.; Jain, P. K.; Ewers, T.; Alivisatos, A. P. Localized Surface Plasmon Resonances Arising from Free Carriers in Doped Quantum Dots. *Nat Mater* **2011**, *10*, 361–366.

(39) Khalakhan, I.; Vorokhta, M.; Xie, X.; Piliai, L.; Matolínová, I. On the Interpretation of X-Ray Photoelectron Spectra of Pt-Cu Bimetallic Alloys. *J Electron Spectros Relat Phenomena* **2021**, *246*, 147027.

(40) Shenasa, M.; Sainkar, S.; Lichtman, D. XPS Study of Some Selected Selenium Compounds. *J Electron Spectros Relat Phenomena* **1986**, *40*, 329–337.

(41) Singh, S.; Tomar, R.; Ten Brinck, S.; De Roo, J.; Geiregat, P.; Martins, J. C.; Infante, I.; Hens, Z. Colloidal CdSe Nanoplatelets, A Model for Surface Chemistry/Optoelectronic Property Relations in Semiconductor Nanocrystals. *J Am Chem Soc* **2018**, *140*, 13292–13300.

(42) Sadtler, B.; Demchenko, D. O.; Zheng, H.; Hughes, S. M.; Merkle, M. G.; Dahmen, U.; Wang, L. W.; Alivisatos, A. P. Selective Facet Reactivity during Cation Exchange in Cadmium Sulfide Nanorods. *J Am Chem Soc* **2009**, *131*, 5285–5293.

(43) White, S. L.; Smith, J. G.; Behl, M.; Jain, P. K. Co-Operativity in a Nanocrystalline Solid-State Transition. *Nat Commun* **2013**, *4*, 2933.

(44) Khammang, A.; Wright, J. T.; Meulenberg, R. W. Mechanistic Insight into Copper Cation Exchange in Cadmium Selenide Semiconductor Nanocrystals Using X-Ray Absorption Spectroscopy. *Nat Commun* **2021**, *12*, 438.

(45) Torres, D. D.; Jain, P. K. Ab Initio Investigation of Cooperativity in Ion Exchange. *J. Phys. Chem. C* **2020**, *124*, 25615–25620.

TOC graphic

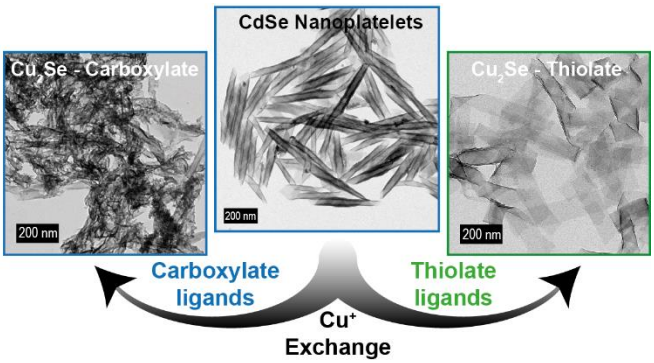
CdSe Nanoplatelets
Cu2Se - Carboxylate
Cu2Se - Thiolate
200 nm
200 nm
200 nm
Carboxylate ligands
Thiolate ligands
Cu+ Exchange